

Scale and redshift dependent limits on cosmic neutrino properties

Deng Wang* and Olga Mena†

Instituto de Física Corpuscular (CSIC-Universitat de València), E-46980 Paterna, Spain

Eleonora Di Valentino‡

*School of Mathematical and Physical Sciences, University of Sheffield,
Hounsfield Road, Sheffield S3 7RH, United Kingdom*

Stefano Gariazzo§

*Department of Physics, University of Turin, via P. Giuria 1, 10125 Turin (TO), Italy and
Istituto Nazionale di Fisica Nucleare (INFN), Sezione di Torino, via P. Giuria 1, 10125 Turin (TO), Italy*

Cosmological neutrino mass and abundance measurements are reaching unprecedented precision. Testing their stability versus redshift and scale is a crucial issue, as it can serve as a guide for optimizing ongoing and future searches. Here, we perform such analyses, considering a number of redshift, scale, and redshift-and-scale nodes. Concerning the k -space analysis of $\sum m_\nu$, CMB observations are crucial, as they lead the neutrino mass constraints. Interestingly, some data combinations suggest a non-zero value for the neutrino mass with 2σ significance. The most constraining bound we find is $\sum m_\nu < 0.54$ eV at 95% CL in the $[10^{-3}, 10^{-2}]$ h/Mpc k -bin, a limit that barely depends on the data combination. Regarding the redshift- and scale-dependent neutrino mass constraints, high redshifts ($z > 100$) and scales in the range $[10^{-3}, 10^{-1}]$ h/Mpc provide the best constraints. The least constraining bounds are obtained at very low redshifts $[0, 0.5]$ and also at very small scales ($k > 0.1$ h/Mpc), due to the absence of observations. Highly relevant is the case of the $[100, 1100]$, $[10^{-2}, 10^{-1}]$ h/Mpc redshift-scale bin, where a 2 – 3σ evidence for a non-zero neutrino mass is obtained for all data combinations. The bound from CMB alone at 68% CL is $0.63^{+0.20}_{-0.24}$ eV, and the one for the full dataset is $0.56^{+0.20}_{-0.23}$ eV, clearly suggesting a non-zero neutrino mass at these scales, possibly related to a deviation of the ISW amplitude in this redshift range. Concerning the analysis of N_{eff} in the k -space, at intermediate scales ranging from $k = 10^{-3}$ h/Mpc to $k = 10^{-1}$ h/Mpc , accurate CMB data provide very strong bounds, the most robust one being $N_{\text{eff}} = 3.09 \pm 0.14$, comparable to the standard expected value without a k -bin analysis. If a non-zero neutrino mass is considered, the bounds on the N_{eff} values at the different k -bins are largely unaffected, and the 95% CL tightest limit we find for the neutrino mass in this case is $\sum m_\nu < 0.205$ eV from the full dataset. Finally, the z and k analyses of N_{eff} indicate a high constraining power of cosmological observations at high redshifts and intermediate scales $[10^{-2}, 10^{-1}]$ h/Mpc when extracting the binned values of this parameter.

I. INTRODUCTION

Cosmological bounds on neutrino masses currently provide the tightest constraints on this fundamental quantity. Its precise value plays a key role not only from a purely theoretical perspective but also in the experimental roadmap, as neutrinoless double beta decay searches, which investigate the possible Majorana nature of neutrinos, depend on the absolute scale of neutrino masses and their hierarchical ordering. While neutrino oscillation experiments have measured two squared-mass differences, $|\Delta m_{31}^2| \equiv |m_3^2 - m_1^2| \simeq 2.5 \cdot 10^{-3} \text{ eV}^2$ and $\Delta m_{21}^2 \equiv m_2^2 - m_1^2 \simeq 7.5 \cdot 10^{-5} \text{ eV}^2$ [1–3], this leads to two possible mass orderings: *normal* ($\Delta m_{31}^2 > 0$) and *inverted* ($\Delta m_{31}^2 < 0$). A number of ongoing and future neutrino oscillation experiments aim to determine

the neutrino mass ordering [4–8]; see also Ref. [9]. Neutrino oscillation experiments provide a lower limit for the total neutrino mass, $\sum m_\nu > 0.06$ eV for NO and $\sum m_\nu > 0.1$ eV for IO [2]. Direct searches in the KATRIN experiment imply $\sum m_\nu < 1.35$ eV [10], where $\sum m_\nu \equiv m_1 + m_2 + m_3$ is the total neutrino mass.

The most constraining cosmological neutrino bound is approaching, or even surpassing, the minimum scale predicted by terrestrial oscillation searches, i.e., around $\sum m_\nu \lesssim 0.05$ eV [11], leading to a tension between oscillation results and cosmological observations [12].¹

On the other hand, the number of neutrino species is commonly parameterized in terms of the effective number

*Electronic address: dengwang@ific.uv.es

†Electronic address: omena@ific.uv.es

‡Electronic address: e.divalentino@sheffield.ac.uk

§Electronic address: stefano.gariazzo@unito.it

¹ Notice that cosmological inferences, however, are indirect. Relaxing the equation of state of dark energy [13–35], the Hubble constant H_0 [36–39], the amplitude parameter σ_8 [36, 40, 41], which are in tension among different datasets [42–47]; CMB lensing [21, 48–54], or allowing new physics in the neutrino sector [55–76] or isolating background from perturbation effects [77] may relax the limit quoted before.

of relativistic degrees of freedom, N_{eff} , by

$$\rho_{\text{R}} = \rho_{\gamma} \left(1 + \frac{7}{8} \left(\frac{4}{11} \right)^{4/3} N_{\text{eff}} \right), \quad (1)$$

where ρ_{γ} represents the photon energy density. Here, N_{eff} includes the contribution of all relativistic particles besides photons. If we consider the simplest three-neutrino case with an instantaneous decoupling process, N_{eff} would be equal to 3. A value $N_{\text{eff}} \neq 3$, however, would be the consequence of either new degrees of freedom unrelated to standard neutrinos, a non-standard momentum distribution for the three neutrinos, or other exotic new physics in the neutrino sector, such as the presence of additional neutrino states [78, 79]. Even in the standard case, the value of N_{eff} deviates from 3 due to non-instantaneous decoupling. This deviation can be computed numerically by considering the full framework of neutrino oscillations, interactions with electrons and positrons, Finite-Temperature corrections to Quantum Electro-Dynamics (FT-QED), and the expansion of the universe, leading to $N_{\text{eff, std}} = 3.044$ [80–84], see also [85, 86]. Current cosmological observations indicate that N_{eff} is close to 3, as measured independently by CMB observations ($N_{\text{eff}} = 2.99^{+0.34}_{-0.33}$ at 95% confidence level (CL) [36]) and BBN abundances (e.g., $N_{\text{eff}} = 2.87^{+0.24}_{-0.21}$ at 68% CL [87]). The above constraints have been shown to be extremely robust against different fiducial cosmologies; see Ref. [17].² Given the fact that neutrinos transition from a purely relativistic radiation component in the early Universe to non-relativistic species (contributing to the Universe’s matter energy density) at late times, it is mandatory to test whether the cosmological measurements of neutrino masses and abundances hold throughout cosmic evolution and to assess the capability of different datasets to constrain both properties at various cosmological scales and times. Redshift-dependent cosmological limits on neutrino masses and abundances have been computed previously in the literature [67, 88]. Here, we go beyond these studies by including an analysis of the stability of cosmological neutrino limits with respect to both *scale* and the combination of *redshift and scale*. We conduct these analyses to gain insight into the constraining power of cosmological datasets regarding neutrino properties, not only as a function of time but also as a function of scale. This will be invaluable for identifying which scales are most sensitive to, e.g., the neutrino mass—crucial information for future cosmological measurements, which are expected to detect the minimum neutrino mass and determine N_{eff} with unprecedented precision [89–92].

The structure of this manuscript is as follows. Section II A contains a description of the datasets employed in this work. Section II B outlines the redshift and scale binning adopted in the numerical analyses, presented in terms of scale, redshift, and the combination of both for neutrino masses and abundances. Section II C details the methodology adopted. We present our results in Sec. III, and finally, we conclude in Sec. IV.

II. DATA, MODELING AND METHODOLOGY

A. Observational data sets

In the following, we describe the datasets used to perform our analysis.

- **CMB.** We consider the Planck 2018 high- ℓ `plik` temperature (TT) likelihood covering multipoles $30 \leq \ell \leq 2508$, polarization (EE), and their cross-correlation (TE) data spanning $30 \leq \ell \leq 1996$. Furthermore, we incorporate the low- ℓ TT `Commander` and `SimAll` EE likelihoods in the range $2 \leq \ell \leq 29$ [93]. In addition, we conservatively include the Planck CMB lensing likelihood derived from `SMICA` maps across $8 \leq \ell \leq 400$ [94], namely `TTTEEE+low ℓ +lowE+lensing` [36, 93, 95, 96]. The Planck datasets are expected to provide constraints covering scales $10^{-4} \lesssim k [h \text{ Mpc}^{-1}] \lesssim 0.3$. Moreover, the CMB originated at redshift $z \simeq 1100$, but the evolution of the Universe has an impact on its spectrum even at much later times. As a consequence, the CMB dataset can probe redshifts down to $z = \mathcal{O}(10)$.
- **MPK.** The galaxy power spectrum is an important quantity for measuring the large-scale structure of the Universe at late times. It can be transformed into the matter power spectrum (MPK) by modeling the so-called galaxy bias. In this analysis, we use the galaxy power spectrum data measured at four effective redshifts, $z_{\text{eff}} = 0.22, 0.41, 0.60, \text{ and } 0.78$, from the WiggleZ Dark Energy Survey [97, 98], which measured 238,000 galaxy redshifts from seven regions of the sky with a total volume of 1 Gpc^3 in the scale range $[0.01, 0.5] h \text{ Mpc}^{-1}$.
- **DESY1.** The Dark Energy Survey Year 1 (DESY1) large-scale structure observations [99–103] include the following three two-point correlation functions:
 1. *Galaxy clustering.* The homogeneity of the matter distribution in the Universe can be traced by the distribution of galaxies. The overabundance of galaxy pairs at an angular separation θ in a random distribution, $\omega(\theta)$, is one of the most convenient ways to measure galaxy clustering. It quantifies the scale

² The largest departure concerning the uncertainties in N_{eff} appears in models that also consider the Helium fraction as a free parameter, due to the degeneracy between N_{eff} and Y_p^{BBN} via the Silk damping effect.

dependence and strength of galaxy clustering and, consequently, affects matter clustering.

2. *Cosmic shear.* The two-point statistics describing galaxy shapes are complex since they result from components of a spin-2 tensor. Thus, it is convenient to extract information from a galaxy survey using a pair of two-point correlation functions, $\xi_+(\theta)$ and $\xi_-(\theta)$, which represent the sum and difference of products of the tangential and cross components of the shear, measured with respect to the line connecting each pair of galaxies.
3. *Galaxy-galaxy lensing.* The typical distortion of source galaxy shapes arises from masses associated with foreground lenses. This distortion is characterized by the mean tangential ellipticity of source galaxy shapes around lens galaxy positions for each pair of redshift bins and is consequently referred to as the tangential shear, $\zeta_t(\theta)$.

DESY1 observations cover the range $0.15 \lesssim z \lesssim 0.9$ for the galaxy samples and $0.2 \lesssim z \lesssim 1.3$ for cosmic shear. Concerning scales, the tested range is approximately $[0.01, 0.5] h \text{ Mpc}^{-1}$.

B. Scale and redshift dependent model

Concerning the *scale-dependent analyses*, we make use of seven k -bins for $\sum m_\nu$ and N_{eff} , namely: $[0, 10^{-4}]$, $[10^{-4}, 10^{-3}]$, $[10^{-3}, 10^{-2}]$, $[10^{-2}, 10^{-1}]$, $[10^{-1}, 1]$, $[1, 10]$, and $[10, +\infty]$, all in h/Mpc units. The parameter values at these nodes are Σm_ν^{k7} , Σm_ν^{k6} , Σm_ν^{k5} , Σm_ν^{k4} , Σm_ν^{k3} , Σm_ν^{k2} , Σm_ν^{k1} , and N_{eff}^{k7} , N_{eff}^{k6} , N_{eff}^{k5} , N_{eff}^{k4} , N_{eff}^{k3} , N_{eff}^{k2} , N_{eff}^{k1} .

Regarding the scale- and redshift-dependent constraints for $\sum m_\nu$, we adopt six redshift bins (i): $[0, 0.5]$, $[0.5, 3]$, $[3, 10]$, $[10, 100]$, $[100, 1100]$, and $[1100, +\infty]$, along with four bins in k -space (j): $[10^{-1}, +\infty]$, $[10^{-2}, 10^{-1}]$, $[10^{-3}, 10^{-2}]$, and $[0, 10^{-3}]$ (all in h/Mpc units). The values of $\sum m_\nu$ at these nodes are Σm_ν^{ij} , with $i = 1, \dots, 6$ and $j = 1, \dots, 4$, leading to a total of 24 additional parameters.

Given that N_{eff} is primarily constrained by recombination physics, we consider only three redshift bins: $[0, 100]$, $[100, 1100]$, and $[1100, +\infty]$, along with three k -space bins: $[10^{-1}, +\infty] h/\text{Mpc}$, $[10^{-2}, 10^{-1}] h/\text{Mpc}$, and $[0, 10^{-2}] h/\text{Mpc}$. The values of N_{eff} at these nodes are N_{eff}^{ij} , with $i = 1, \dots, 3$ and $j = 1, \dots, 3$, resulting in a total of 9 new parameters.

C. Analysis methodology

In order to calculate the theoretical power spectra and the background evolution of the Universe, we use the

Boltzmann solver CAMB [104]. For the Bayesian analysis, we employ the Monte Carlo Markov Chain (MCMC) method to infer the posterior distributions of model parameters, leveraging the publicly available package CosmoMC [105, 106]. We assess the convergence of the MCMC chains via the Gelman-Rubin statistic criterion, requiring $R-1 \lesssim 0.05$ [107], and analyze the chains using the package Getdist [108].

We use the following uniform priors for the model parameters: the baryon fraction $\Omega_b h^2 \in [0.005, 0.1]$, the cold dark matter fraction $\Omega_c h^2 \in [0.001, 0.99]$, the acoustic angular scale at the recombination epoch $100\theta_{MC} \in [0.5, 10]$, the scalar spectral index $n_s \in [0.8, 1.2]$, the amplitude of the primordial scalar power spectrum $\ln(10^{10} A_s) \in [2, 4]$, the optical depth $\tau \in [0.01, 0.8]$, and the sum of the masses of the three active neutrinos $\sum m_\nu \in [0, 5] \text{ eV}$. For the scale-dependent neutrino mass model, we use the prior $\sum m_\nu^{ki} \in [0, 30] \text{ eV}$ with $i = 1, \dots, 7$ in each k -bin. For the scale- and redshift-dependent neutrino mass model, we use the prior $\sum m_\nu^{ij} \in [0, 30] \text{ eV}$ with $i = 1, \dots, 6$ and $j = 1, \dots, 4$ in each bin. For the scale-dependent number of relativistic species model, both without and with massive neutrinos, we use the prior $N_{\text{eff}}^{ki} \in [0, 30]$ with $i = 1, \dots, 7$ in each k -bin. For the scale- and redshift-dependent number of relativistic species model, we use the prior $N_{\text{eff}}^{ij} \in [0, 30]$ with $i = 1, \dots, 3$ and $j = 1, \dots, 3$ in each bin. We adopt the degenerate neutrino hierarchy throughout this study.

III. RESULTS

A. Scale and redshift dependent neutrino mass limits

Table 1 shows the constraints on the main cosmological parameters, as well as on the different values of $\sum m_\nu$ at the corresponding bins in k -space. Notice that Σm_ν^{k7} , corresponding to very large scales, is poorly constrained regardless of the datasets used in the analyses. The lack of observational measurements at these very large scales leads to a very loose bound on this parameter. The situation changes completely when moving to the next two k -bins, i.e., the $[10^{-4}, 10^{-3}] h/\text{Mpc}$ and the $[10^{-3}, 10^{-2}] h/\text{Mpc}$ bins. Here, CMB observations are crucial, as they dominate the neutrino mass constraints, as can also be inferred from Figs. 1 and 2: the additional datasets related to large-scale structure data do not further improve the bounds on either Σm_ν^{k6} or Σm_ν^{k5} . The following two bins are particularly interesting, as some data combinations suggest a non-zero value for the neutrino mass. More concretely, within the $[10^{-2}, 10^{-1}] h/\text{Mpc}$ k -bin, the CMB plus DESY1 datasets together provide the bound $\Sigma m_\nu^{k5} = 0.55 \pm 0.26 \text{ eV}$ with 68% CL errors, indicating a non-zero neutrino mass at the 2σ significance level (see also Fig. 2). For the rest of the data combinations, the limit on Σm_ν^{k5} remains very similar to the CMB-only result. For the

Σm_ν^{k4} parameter, associated with the $[10^{-1}, 1]$ h/Mpc k -bin, the situation is different: in general, the addition of large-scale structure data significantly alters the CMB-only limit, as these scales play a leading role in constraining neutrino mass. For instance, the addition of DESY1 measurements to CMB changes the 95% CL upper bound on Σm_ν^{k3} from 2.30 eV to 0.82 eV. When adding MPK observations to CMB, we find $\sim 3\sigma$ evidence for a non-zero neutrino mass, $\Sigma m_\nu^{k3} = 1.02 \pm 0.36$ eV. For the full dataset combination (CMB plus DESY1 plus MPK), we obtain $\Sigma m_\nu^{k3} = 0.75^{+0.31}_{-0.41}$ eV, suggesting a non-zero value for the neutrino mass with 2σ significance. Within the remaining bins in k -space, corresponding to very small scales, the neutrino mass is largely unconstrained, except in a few cases where DESY1 data are considered along with other datasets. Specifically, DESY1 marginally contributes in these cases. For instance, we obtain $\Sigma m_\nu^{k2} < 18.70$ eV at 95% CL for the $[1, 10]$ h/Mpc k -bin.

The redshift- and scale-dependent neutrino mass constraints are depicted in Tab. II. Notice that, at the highest redshift bin, $z > 1100$, the CMB constraining power on neutrino masses barely changes when considering additional datasets, which cannot probe such high redshift values. Only in the k -range $[10^{-2}, 10^{-1}]$ h/Mpc are these additional measurements mildly significant: for instance, the 95% CL upper limit on Σm_ν^{62} of 0.85 eV from CMB data alone is shifted down to 0.79 eV when also including the MPK dataset. For smaller scales, the bound on Σm_ν^{61} of 3.50 eV from CMB data alone remains unchanged when incorporating large-scale structure constraints, due to the lack of precise large-scale structure measurements in the $[10^{-1}, +\infty]$ h/Mpc k -bin, where non-linearities are crucial.

The $[100, 1100]$ redshift range also benefits from large-scale structure measurements, especially in the $[10^{-3}, 10^{-2}]$ h/Mpc and $[10^{-2}, 10^{-1}]$ h/Mpc k -bins. Highly relevant is the case of Σm_ν^{52} , where a 2 – 2.5σ evidence for a non-zero neutrino mass is obtained for all data combinations. The bound from CMB alone is $0.63^{+0.20}_{-0.24}$ eV, while the bound for the full dataset combination (CMB plus DESY1 plus MPK) is $0.56^{+0.20}_{-0.23}$ eV, clearly suggesting a non-zero neutrino mass at these scales within the $[100, 1100]$ redshift range. This signal could be related to the fact that there is a $\sim 2\sigma$ deviation of the ISW amplitude ($A_{\text{ISW}} > 1$) at redshift $z = 500$, as indicated by the tomographic analyses of Ref. [109]. Since neutrino masses reduce the ISW effect, a relatively large neutrino mass (compared to the current cosmological limits) could, in principle, compensate for such an effect.

For the $[10, 100]$ redshift bin, the tightest constraints are found within the $[10^{-3}, 10^{-2}]$ h/Mpc k -bin, where CMB measurements are highly relevant and dominant: the CMB-only limit of $\Sigma m_\nu^{43} < 1.11$ eV at 95% CL does not change when additional measurements are considered. At the smallest scales, the neutrino mass is unconstrained—i.e., no limit on Σm_ν^{41} is found—while the

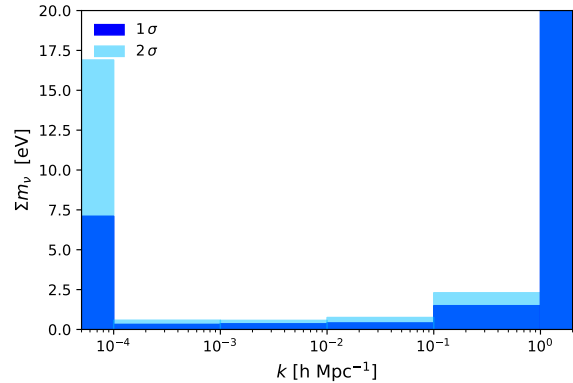


FIG. 1: The tomographic reconstruction of neutrino masses across cosmic scales from CMB data.

limits on Σm_ν^{42} are also very weak. The situation in the following redshift bin, $[3, 10]$, is very similar, although in this case the CMB-only limit is higher: $\Sigma m_\nu^{33} < 3.10$ eV at 95% CL. It is precisely in the $[0.5, 3]$ redshift range where the effects of large-scale structure data become relevant, especially within the $[10^{-2}, 10^{-1}]$ h/Mpc k -bin. The 95% CL limit on $\Sigma m_\nu^{22} < 5.90$ eV from CMB data alone is reduced to $2.20^{+1.00}_{-1.50}$ eV when the full dataset combination is considered. Even more interesting is the case of Σm_ν^{21} , which is completely unconstrained by CMB observations but gains constraints at 95% CL of 3.20 eV and 5.00 eV when adding DESY1 and MPK measurements to CMB data, respectively. When considering the full dataset, we obtain $\Sigma m_\nu^{21} = 2.15^{+0.95}_{-1.40}$ eV, indicating a very mild preference for a non-zero neutrino mass. The lowest redshift range provides very weak constraints on the neutrino mass, especially at the highest and lowest scales. Only the value of Σm_ν^{13} is always constrained, albeit very poorly. The lack of observations in these ranges leads to very weak bounds on the neutrino mass.

Figure 3 depicts the results for the neutrino mass constraints as a function of redshift and k -bins. Notice that high redshifts ($z > 100$) and scales in the range $[10^{-3}, 10^{-1}]$ h/Mpc provide the best constraints. The least constraining bounds are obtained at very low redshifts, $[0, 0.5]$, and at very small scales ($k > 0.1$ h/Mpc), due to the absence of observations. In this particular region of k -space, a bound on the neutrino mass is found only if $z > 100$.

B. Scale and redshift dependent constraints on N_{eff}

Table III and Fig. 4 show the constraints on N_{eff} at the different k -bins considered here, assuming a vanishing neutrino mass. At the largest scales, $[0, 10^{-4}]$ h/Mpc , the lack of observations leads to a completely unconstrained value of N_{eff}^{k7} . A very similar situation occurs for the $[10^{-4}, 10^{-3}]$ h/Mpc k -bin, where only a very loose

TABLE I: Mean values and 1σ (68%) marginalized errors of the cosmological parameters within the scale-dependent neutrino mass model, obtained using the CMB, CMB plus DESY1, CMB plus MPK, and CMB plus DESY1 plus MPK datasets, respectively. Note that we quote 2σ (95% CL) limits for parameters that cannot be measured by the data. The symbols “★” denote parameters that remain unconstrained by the data.

Parameters	CMB	CMB+DESY1	CMB+MPK	CMB+DESY1+MPK
$\Omega_b h^2$	0.02242 ± 0.00015	0.02249 ± 0.00014	0.02240 ± 0.00014	0.02246 ± 0.00014
$\Omega_c h^2$	0.1196 ± 0.0012	0.1186 ± 0.0011	0.1199 ± 0.0011	$0.1189^{+0.0011}_{-0.00099}$
$100\theta_{MC}$	1.04091 ± 0.00031	1.04100 ± 0.00031	1.04087 ± 0.00031	1.04098 ± 0.00030
τ	0.0545 ± 0.0075	0.0550 ± 0.0076	0.0530 ± 0.0073	0.0543 ± 0.0071
$\ln(10^{10} A_s)$	3.045 ± 0.015	3.044 ± 0.015	3.042 ± 0.014	3.043 ± 0.014
n_s	0.9663 ± 0.0044	0.9668 ± 0.0042	0.9651 ± 0.0040	0.9665 ± 0.0040
Σm_ν^{k1}	★	> 7.23	★	★
Σm_ν^{k2}	★	★	★	< 19.9
Σm_ν^{k3}	< 2.28	< 0.806	1.02 ± 0.36	$0.75^{+0.31}_{-0.41}$
Σm_ν^{k4}	< 0.744	0.55 ± 0.26	< 0.761	< 0.875
Σm_ν^{k5}	< 0.563	< 0.570	< 0.574	< 0.542
Σm_ν^{k6}	< 0.572	< 0.552	< 0.563	< 0.560
Σm_ν^{k7}	< 16.5	< 18.1	< 17.7	< 17.6
H_0	67.60 ± 0.55	68.06 ± 0.51	67.45 ± 0.49	$67.90^{+0.45}_{-0.50}$
Ω_m	0.3123 ± 0.0075	0.3060 ± 0.0067	0.3144 ± 0.0067	0.3082 ± 0.0064
σ_8	$0.771^{+0.025}_{-0.022}$	$0.787^{+0.015}_{-0.010}$	$0.771^{+0.018}_{-0.016}$	$0.775^{+0.020}_{-0.016}$
S_8	0.787 ± 0.025	$0.794^{+0.017}_{-0.014}$	0.789 ± 0.020	$0.785^{+0.021}_{-0.019}$

upper bound of ~ 8 is found. For intermediate scales, ranging from $k = 10^{-3} h/\text{Mpc}$ to $k = 10^{-1} h/\text{Mpc}$, accurate CMB data provide very strong constraints (with additional datasets barely improving the CMB bounds), especially in the cases of N_{eff}^{k4} and N_{eff}^{k3} , where the error is slightly smaller than in the N_{eff}^{k5} case. The bound on N_{eff}^{k4} in the full dataset combination yields $N_{\text{eff}}^{k4} = 3.09 \pm 0.14$, with an uncertainty comparable to the standard expected value without a k -bin analysis. Interestingly, within the $[10^{-3}, 10^{-2}] h/\text{Mpc}$ k -bin, the mean value of N_{eff} is below 3, while in the next two k -bins, the mean value is always above 3. At the smallest scales, N_{eff} remains unconstrained, except for N_{eff}^{k2} , associated with the $[1, 10] h/\text{Mpc}$ k -bin, where the addition of DESY1 and/or MPK data provides limits (see associated panel in Fig. 4), with the mean value of N_{eff} in these cases also falling below 3. A complete and straightforward picture of the overall analysis is provided by Fig. 5, where the strong constraining power of CMB data at scales between $k = 10^{-3} h/\text{Mpc}$ and $k = 10^{-1} h/\text{Mpc}$ is clearly evident.

Table IV and Fig. 6 show the analysis for different k nodes in N_{eff} , assuming a non-vanishing neutrino mass. While at the largest scales, $[0, 10^{-4}] h/\text{Mpc}$, the situation is very similar to that of massless neutrinos—leading to a completely unconstrained value of N_{eff}^{k7} —a very different

scenario arises in the $[10^{-4}, 10^{-3}] h/\text{Mpc}$ k -bin, where a non-zero value for N_{eff} is found (despite the large errors). For the other k -bins, the results closely resemble those of the massless neutrino case, except for N_{eff}^{k1} and N_{eff}^{k2} in the CMB + DESY1 data combination, where no limits are found—unlike in the massless neutrino case.

Indeed, the tightest bound is still found for $N_{\text{eff}}^{k4} = 3.10 \pm 0.14$ for the full dataset combination. Concerning the neutrino mass bound, it is naturally higher than in the standard three-massive-neutrino case, due (to a minor extent) to degeneracies with N_{eff} and (to a larger extent) to the much wider neutrino parameter space. Nevertheless, the 95% CL limit we find here, $\Sigma m_\nu < 0.205$ eV from the full dataset, is comparable to those found in minimally extended cosmologies. See, for instance, the constraints reported by Ref. [17] in extended neutrino cosmologies.

Finally, we shall perform a modest redshift- and k -dependent analysis on N_{eff} . In the following, we consider three redshift bins in each z and k space, constraining the following parameters: N_{eff}^{11} , with z in $[0, 100]$ and k in $[10^{-1}, +\infty] h/\text{Mpc}$; N_{eff}^{12} , with z in $[0, 100]$ and k in $[10^{-2}, 10^{-1}] h/\text{Mpc}$; N_{eff}^{13} , with z in $[0, 100]$ and k in $[0, 10^{-2}]$; N_{eff}^{21} , with z in $[100, 1100]$ and k in $[10^{-1}, +\infty] h/\text{Mpc}$; N_{eff}^{22} , with z in $[100, 1100]$ and

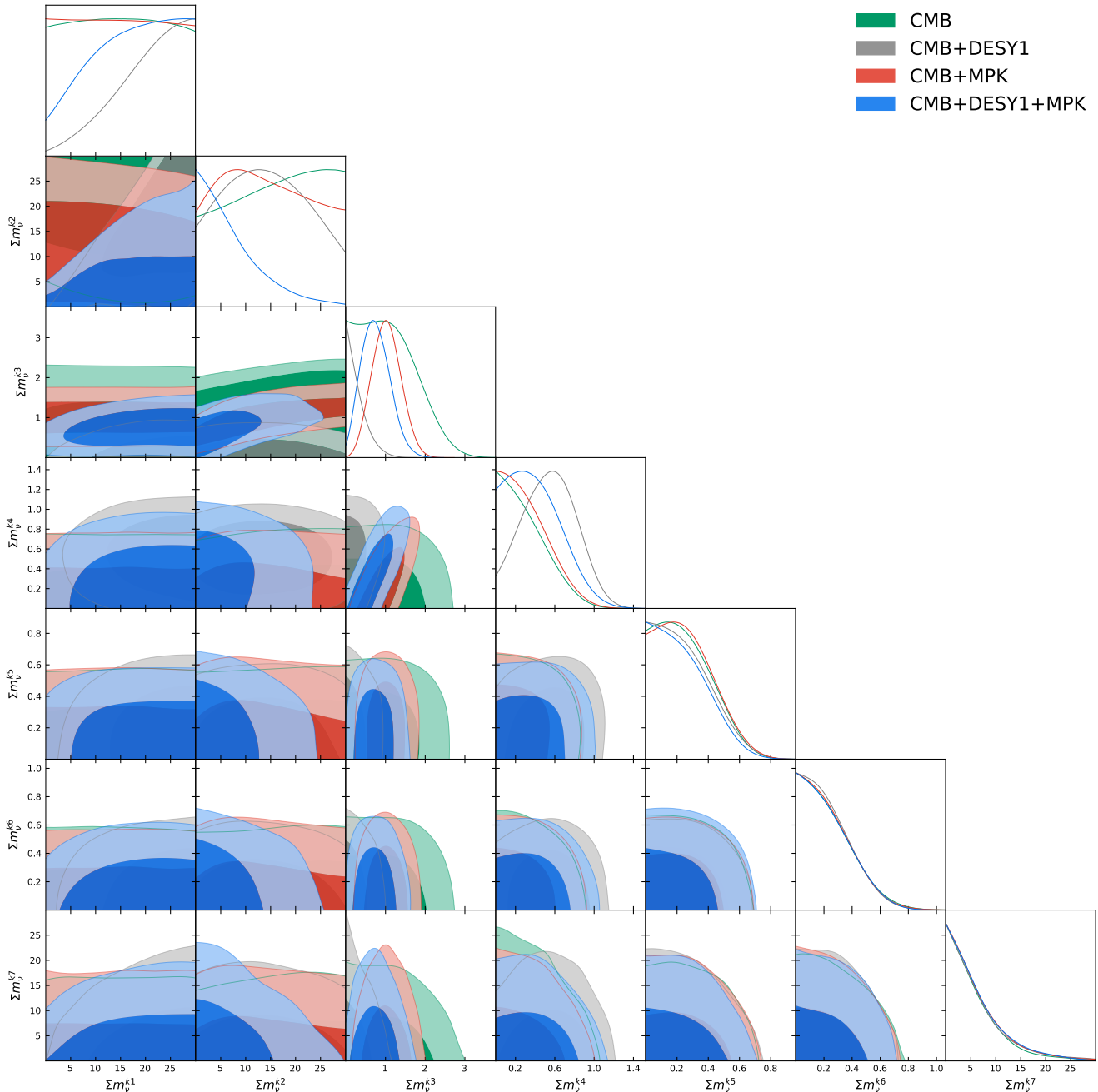


FIG. 2: One-dimensional and two-dimensional marginalized constraints on the scale-dependent neutrino mass model from CMB, CMB plus DES Y1, CMB plus MPK and CMB plus DES Y1 plus MPK datasets, respectively.

k in $[10^{-2}, 10^{-1}]$ h/Mpc ; N_{eff}^{23} , with z in $[100, 1100]$ and k in $[0, 10^{-2}]$; N_{eff}^{31} , with z in $[1100, +\infty]$ and k in $[10^{-1}, +\infty]$ h/Mpc ; N_{eff}^{32} , with z in $[1100, +\infty]$ and k in $[10^{-2}, 10^{-1}]$ h/Mpc ; and N_{eff}^{33} , with z in $[1100, +\infty]$ and k in $[0, 10^{-2}]$ h/Mpc . Table V and Fig. 7 show the results for these two-parameter bin analyses, assuming massless neutrinos. The best constraints are found in the two redshift bins $[100, 1100]$ and $[1100, +\infty]$, due to the precision of CMB data within these two redshift

bins, with errors very close to those found in the standard case for k -bins in $[10^{-2}, 10^{-1}]$ h/Mpc and also k within $[0, 10^{-2}]$ h/Mpc . The most constraining extraction of N_{eff} is $N_{\text{eff}}^{22} = 3.14 \pm 0.15$. Notice also that for the largest scales, i.e., k in the $[0, 10^{-2}]$ h/Mpc bin, the mean value of N_{eff} is always very close to or below 3, probably suggesting a lower damping induced by N_{eff} at these scales. For the lowest redshift bin, N_{eff} is, in practice, unconstrained or constrained with very loose bounds. The

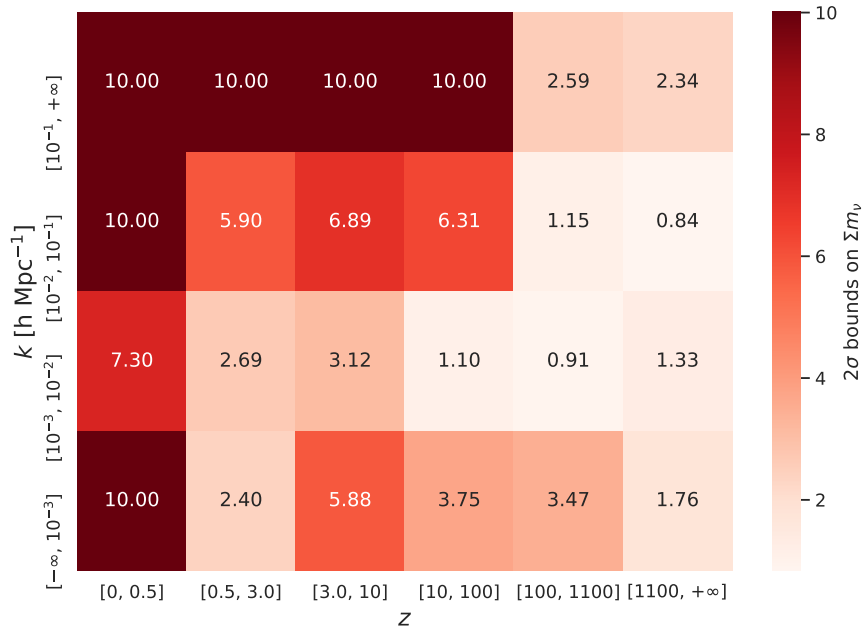


FIG. 3: 2σ bounds on neutrino masses in the redshift- and scale-dependent neutrino mass model from CMB data. Note that all bins have 2σ upper bounds except for Σm_ν^{64} , which has a 2σ lower limit of 1.76 eV. The value “10.00” denotes parameters that remain unconstrained by the data.

tomographic z - and k -reconstruction of N_{eff} is depicted in Fig. 8, where the high constraining power of high redshifts and intermediate scales ($[10^{-2}, 10^{-1}]$ h/Mpc) is clearly noticeable.

IV. SUMMARY

Neutrinos are hot thermal relics with very large velocity dispersions and therefore undergo a transition from a purely relativistic component to a non-relativistic one. Given the particular nature of neutrinos, it is essential to explore the redshift- and scale-dependent limits on both neutrino masses and abundances. While redshift-dependent cosmological limits on neutrino masses and abundances have been computed previously in the literature, see e.g., Refs. [67, 88], we include here the cosmological neutrino limits versus *scale* and also versus both *redshift and scale*. We make use of a variety of cosmological observations, namely CMB, MPK, and DESY1 data. From the reconstruction of the neutrino mass as a function of scale, we find that this parameter is poorly constrained at very large scales, regardless of the datasets used in the analyses. The situation changes completely within the $[10^{-4}, 10^{-3}]$ h/Mpc and $[10^{-3}, 10^{-2}]$ h/Mpc bins, where CMB observations play a crucial role. Within the $[10^{-2}, 10^{-1}]$ h/Mpc k -bin, the CMB plus DESY1 datasets together provide

the bound $\Sigma m_\nu^{k5} = 0.55 \pm 0.26$ eV with 68% CL errors, indicating a non-zero neutrino mass with a 2σ significance level. When focusing on redshift- and scale-dependent neutrino mass constraints, an extremely exciting result is found: within the $[100, 1100]$ redshift range and the $[10^{-2}, 10^{-1}]$ h/Mpc k -bin, a non-zero neutrino mass is obtained for all data combinations, with $\Sigma m_\nu^{52} = 0.63_{-0.24}^{+0.20}$ eV from CMB data alone, indicating a $2\text{--}3\sigma$ evidence for massive neutrinos at these redshifts and scales. This anomaly could be related to the observed deviation of the ISW amplitude, located precisely at these redshifts [109]. On the other hand, assuming a vanishing neutrino mass, a k -space analysis of N_{eff} shows that at the largest scales, $[0, 10^{-4}]$ h/Mpc and $[10^{-4}, 10^{-3}]$ h/Mpc, this parameter is, in practice, unconstrained. Constraints at scales from $k = 10^{-3}$ h/Mpc to $k = 10^{-1}$ h/Mpc are found due to the high precision of CMB observations. The most constraining bound we find is $N_{\text{eff}}^{k4} = 3.09 \pm 0.14$. This measurement is very close to the one obtained in the standard case. At the smallest scales, N_{eff} is unconstrained, except for N_{eff}^{k2} , associated with the $[1, 10]$ h/Mpc k -bin, where only the addition of DESY1 and/or MPK data allows for meaningful limits. For a non-vanishing neutrino mass, the situation is very similar to that of massless neutrinos, except for the $[10^{-4}, 10^{-3}]$ h/Mpc k -bin, where a mean value for N_{eff} is found. The 95% CL upper limit we find on the neutrino mass is $\Sigma m_\nu < 0.205$ eV from the full dataset. Finally,

TABLE II: Mean values and 1σ (68%) marginalized errors of the cosmological parameters within the redshift- and scale-dependent neutrino mass model, obtained using the CMB, CMB plus DESY1, CMB plus MPK and CMB plus DESY1 plus MPK datasets, respectively. Note that we quote 2σ (95% CL) limits for parameters that cannot be measured by the data. The symbols “★” denote parameters that remain unconstrained by the data.

Parameters	CMB	CMB+DESY1	CMB+MPK	CMB+DESY1+MPK
$\Omega_b h^2$	0.02245 ± 0.00019	0.02253 ± 0.00018	0.02245 ± 0.00019	0.02254 ± 0.00018
$\Omega_c h^2$	0.1226 ± 0.0016	0.1207 ± 0.0014	0.1226 ± 0.0015	0.1209 ± 0.0013
$100\theta_{MC}$	1.04063 ± 0.00032	1.04081 ± 0.00032	1.04064 ± 0.00032	1.04081 ± 0.00031
τ	$0.0577^{+0.0077}_{-0.0087}$	0.0603 ± 0.0082	0.0571 ± 0.0083	$0.0602^{+0.0074}_{-0.0083}$
$\ln(10^{10} A_s)$	3.061 ± 0.016	3.062 ± 0.016	3.059 ± 0.016	$3.061^{+0.014}_{-0.016}$
n_s	0.9574 ± 0.0059	0.9613 ± 0.0057	0.9579 ± 0.0057	0.9619 ± 0.0052
Σm_ν^{11}	★	$6.40^{+2.80}_{-1.60}$	$3.70^{+1.20}_{-3.10}$	5.1 ± 2.2
Σm_ν^{12}	★	$6.10^{+2.20}_{-1.70}$	< 8.30	4.9 ± 2.3
Σm_ν^{13}	< 7.30	< 5.10	< 8.20	< 6.70
Σm_ν^{14}	★	★	★	★
Σm_ν^{21}	★	< 3.20	< 5.00	$2.15^{+0.95}_{-1.40}$
Σm_ν^{22}	< 5.90	$2.42^{+0.86}_{-1.20}$	< 4.90	$2.20^{+1.00}_{-1.50}$
Σm_ν^{23}	< 2.69	< 2.30	< 2.80	< 2.50
Σm_ν^{24}	< 2.40	< 2.45	< 2.53	< 2.50
Σm_ν^{31}	★	★	★	★
Σm_ν^{32}	< 6.89	< 5.00	< 7.10	< 5.20
Σm_ν^{33}	< 3.12	< 3.20	< 3.20	< 3.30
Σm_ν^{34}	< 5.88	$3.10^{+1.50}_{-1.80}$	< 6.00	< 5.90
Σm_ν^{41}	★	★	★	$4.7^{+5.0}_{-4.5}$
Σm_ν^{42}	< 6.31	< 5.60	< 6.40	< 5.60
Σm_ν^{43}	< 1.10	< 1.23	< 1.16	< 1.09
Σm_ν^{44}	< 3.75	< 3.60	< 3.70	< 3.50
Σm_ν^{51}	< 2.59	< 2.70	< 2.90	< 2.70
Σm_ν^{52}	$0.63^{+0.20}_{-0.24}$	$0.57^{+0.22}_{-0.26}$	0.61 ± 0.23	$0.56^{+0.20}_{-0.23}$
Σm_ν^{53}	< 0.912	< 0.90	< 0.88	< 0.86
Σm_ν^{54}	< 3.47	< 3.60	< 3.50	< 3.50
Σm_ν^{61}	< 2.34	< 2.40	< 2.50	< 2.40
Σm_ν^{62}	< 0.838	< 0.86	< 0.79	< 0.82
Σm_ν^{63}	< 1.33	$0.65^{+0.32}_{-0.41}$	0.69 ± 0.35	$0.62^{+0.29}_{-0.37}$
Σm_ν^{64}	> 1.76	> 1.10	> 1.40	> 0.80
H_0	66.49 ± 0.66	67.26 ± 0.58	66.49 ± 0.62	67.23 ± 0.56
Ω_m	$0.3298^{+0.0092}_{-0.011}$	0.3183 ± 0.0083	$0.3298^{+0.0087}_{-0.0098}$	$0.3188^{+0.0075}_{-0.0084}$
σ_8	$0.612^{+0.073}_{-0.088}$	$0.554^{+0.031}_{-0.072}$	$0.657^{+0.13}_{-0.066}$	$0.594^{+0.060}_{-0.096}$
S_8	$0.642^{+0.078}_{-0.092}$	$0.570^{+0.034}_{-0.074}$	$0.689^{+0.13}_{-0.074}$	$0.612^{+0.063}_{-0.097}$

we also present a joint redshift- and k -dependent analysis of N_{eff} , with three bins in both z and k , i.e., 9 new pa-

TABLE III: Mean values and 1σ (68%) marginalized errors of the cosmological parameters within the scale-dependent number of relativistic species model without massive neutrinos, obtained using the CMB, CMB plus DESY1, CMB plus MPK, and CMB plus DESY1 plus MPK datasets, respectively. Note that we quote 2σ (95%) limits for parameters that the data cannot constrain well. The symbols “★” denote parameters that remain unconstrained by the data.

Parameters	CMB	CMB+DESY1	CMB+MPK	CMB+DESY1+MPK
$\Omega_b h^2$	0.02249 ± 0.00016	0.02255 ± 0.00015	0.02243 ± 0.00016	0.02251 ± 0.00015
$\Omega_c h^2$	0.1193 ± 0.0021	0.1177 ± 0.0018	0.1208 ± 0.0020	0.1191 ± 0.0017
$100\theta_{MC}$	1.04101 ± 0.00038	1.04119 ± 0.00037	1.04083 ± 0.00037	1.04102 ± 0.00035
τ	0.0519 ± 0.0080	0.0536 ± 0.0078	0.0529 ± 0.0078	0.0540 ± 0.0077
$\ln(10^{10} A_s)$	3.043 ± 0.024	3.035 ± 0.023	3.055 ± 0.023	3.048 ± 0.023
n_s	0.9703 ± 0.0068	0.9695 ± 0.0068	0.9697 ± 0.0069	0.9703 ± 0.0067
N_{eff}^{k1}	★	< 9.17	★	< 4.08
N_{eff}^{k2}	★	> 2.0	2.73 ± 0.75	$2.92_{-0.69}^{+0.56}$
N_{eff}^{k3}	3.10 ± 0.15	3.03 ± 0.15	3.16 ± 0.15	3.10 ± 0.14
N_{eff}^{k4}	3.09 ± 0.15	3.03 ± 0.14	3.14 ± 0.14	3.09 ± 0.14
N_{eff}^{k5}	2.91 ± 0.24	2.85 ± 0.23	2.94 ± 0.23	2.88 ± 0.23
N_{eff}^{k6}	< 7.84	< 7.80	< 8.05	< 8.50
N_{eff}^{k7}	★	★	★	★
H_0	68.26 ± 0.87	68.93 ± 0.77	67.59 ± 0.80	68.34 ± 0.70
Ω_m	0.305 ± 0.012	$0.2954_{-0.0110}^{+0.0097}$	0.314 ± 0.012	0.3033 ± 0.0098
σ_8	0.815 ± 0.012	0.816 ± 0.012	0.816 ± 0.012	0.816 ± 0.011
S_8	0.821 ± 0.014	0.810 ± 0.012	0.835 ± 0.014	0.820 ± 0.012

rameters in total, assuming massless neutrinos. The best constraints are found in the two redshift bins $[100, 1100]$ and $[1100, +\infty]$, due to the precision of CMB data within these two redshift bins, for k -bins in $[10^{-2}, 10^{-1}] h/\text{Mpc}$ and also k in $[0, 10^{-2}] h/\text{Mpc}$. The most constraining extraction of N_{eff} is $N_{\text{eff}}^{22} = 3.14 \pm 0.15$, with errors very close to those found in the standard case. It is very interesting to notice that, while for N_{eff} we can have a specific bin where the constraint is very similar to the one obtained for the standard scenario (no scale or redshift dependence), for the neutrino mass bounds this does not happen. The synergy among the different experiments at different redshifts and scales is what allows one to put a much stronger bound when Σm_ν is assumed to be constant, with more than a factor 10 gain with respect to the bounds obtained on the separate bins. In this light, the results presented here serve as a guide for ongoing and future analyses of CMB and large-scale structure observations at different redshifts and scales and will be instrumental in maximizing the science output in the search for constraints on neutrino properties.

Acknowledgments

DW is supported by the CDEIGENT Fellowship of Consejo Superior de Investigaciones Científicas (CSIC). OM acknowledges the financial support from the MCIU with funding from the European Union NextGenerationEU (PRTR-C17.I01) and Generalitat Valenciana (ASFAE/2022/020). EDV is supported by a Royal Society Dorothy Hodgkin Research Fellowship. S.G. is supported by the Research grant TAsP (Theoretical Astroparticle Physics) funded by Istituto Nazionale di Fisica Nucleare (INFN). This work has been supported by the Spanish MCIN/AEI/10.13039/501100011033 grants PID2020-113644GB-I00 and by the European ITN project HIDDeN (H2020-MSCA-ITN-2019/860881-HIDDeN) and SE project ASYMMETRY (HORIZON-MSCA-2021-SE-01/101086085-ASYMMETRY) and well as by the Generalitat Valenciana grants PROMETEO/2019/083 and CIPROM/2022/69. This article is based upon work from COST Action CA21136 Addressing observational tensions in cosmology with systematics and fundamental physics (CosmoVerse) supported by COST (European Cooperation in Science and Technology). OM acknowledges the financial support from the MCIU with funding from the European Union NextGen-

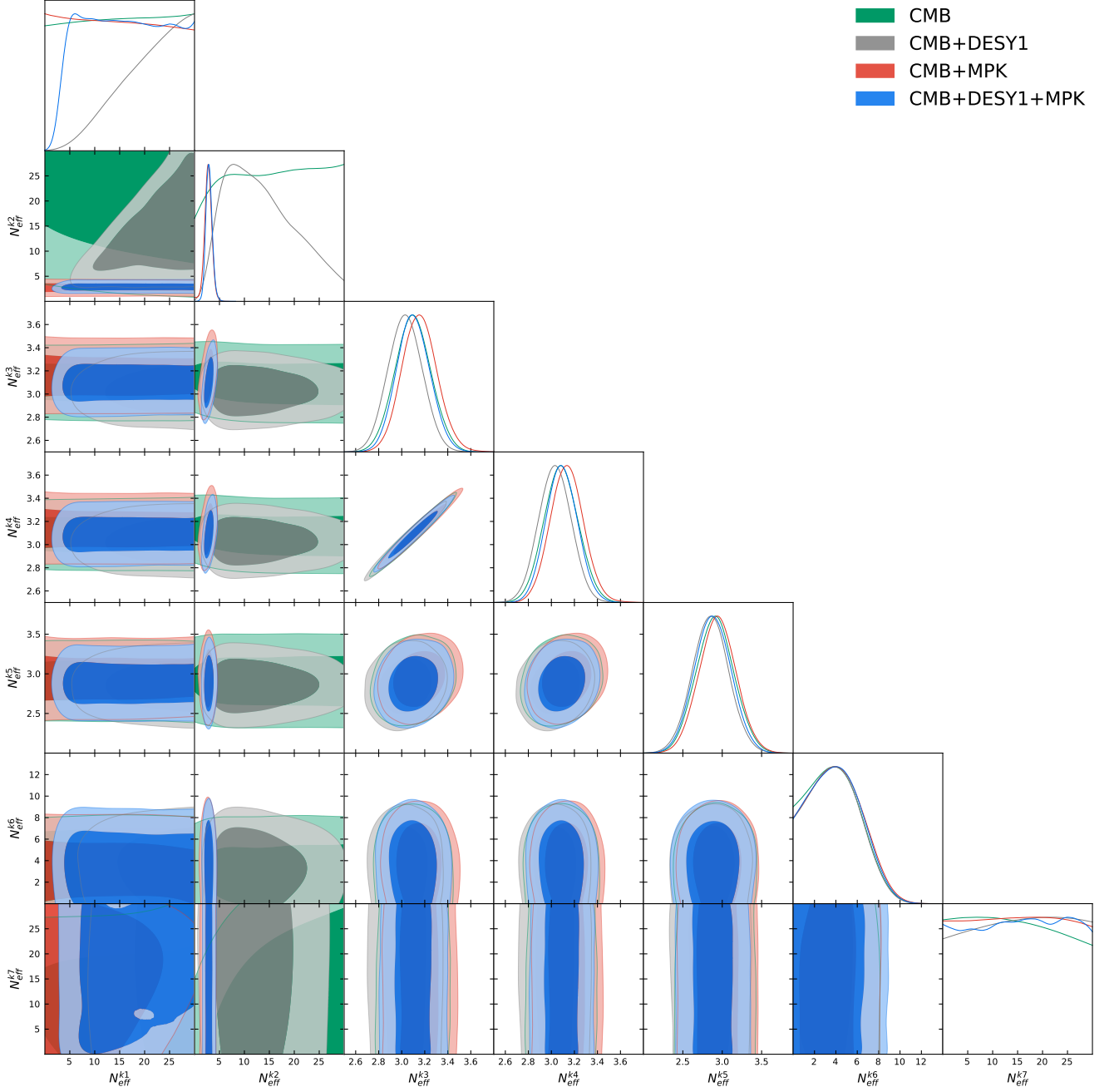


FIG. 4: One-dimensional and two-dimensional marginalized constraints on the scale-dependent number of relativistic species model without massive neutrinos from CMB, CMB plus DESY1, CMB plus MPK and CMB plus DESY1 plus MPK datasets, respectively.

erationEU (PRTR-C17.I01) and Generalitat Valenciana (ASFAE/2022/020).

[1] P. F. de Salas, D. V. Forero, S. Gariazzo, P. Martínez-Miravé, O. Mena, C. A. Ternes, M. Tórtola, and J. W. F. Valle, *JHEP* **02**, 071 (2021), arXiv:2006.11237 [hep-ph].

[2] I. Esteban, M. C. Gonzalez-Garcia, M. Maltoni, I. Martinez-Soler, J. a. P. Pinheiro, and T. Schwetz, (2024), arXiv:2410.05380 [hep-ph].

[3] F. Capozzi, W. Giarè, E. Lisi, A. Marrone, A. Mel-

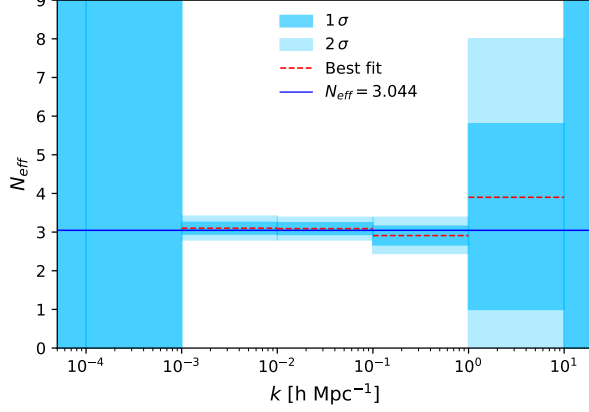


FIG. 5: The tomographic reconstructions of the number of relativistic species across cosmic scales from CMB data. The blue lines denote the standard prediction of $N_{\text{eff}} = 3.044$, and the red dashed lines represent the best fit corresponding to the mean value of posterior distribution in each bin.

TABLE IV: Mean values and 1σ (68%) marginalized errors of the cosmological parameters within the scale-dependent number of relativistic species model with free neutrino mass, obtained using the CMB, CMB plus DESY1, CMB plus MPK and CMB plus DESY1 plus MPK datasets, respectively. Note that we quote 2σ (95%) limits for parameters that the data cannot constrain well. The symbols “★” denote parameters that remain unconstrained by the data.

Parameters	CMB	CMB+DESY1	CMB+MPK	CMB+DESY1+MPK
$\Omega_b h^2$	0.02242 ± 0.00017	0.02250 ± 0.00016	0.02241 ± 0.00017	0.02249 ± 0.00016
$\Omega_c h^2$	$0.1209^{+0.0022}_{-0.0025}$	0.1186 ± 0.0019	0.1214 ± 0.0022	0.1194 ± 0.0018
$100\theta_{MC}$	1.04075 ± 0.00043	1.04102 ± 0.00038	1.04074 ± 0.00039	1.04094 ± 0.00036
τ	0.0531 ± 0.0078	0.0547 ± 0.0079	0.0536 ± 0.0077	0.0551 ± 0.0078
$\ln(10^{10} A_s)$	3.056 ± 0.027	3.044 ± 0.024	3.061 ± 0.025	3.052 ± 0.023
n_s	0.9695 ± 0.0069	0.9690 ± 0.0067	0.9698 ± 0.0071	0.9700 ± 0.0069
Σm_ν	< 0.445	< 0.314	< 0.242	< 0.205
N_{eff}^{k1}	★	★	★	> 4.31
N_{eff}^{k2}	★	★	$2.69^{+0.92}_{-0.61}$	$2.97^{+0.59}_{-0.69}$
N_{eff}^{k3}	3.15 ± 0.16	3.06 ± 0.14	3.18 ± 0.16	3.11 ± 0.15
N_{eff}^{k4}	3.14 ± 0.15	3.06 ± 0.14	3.16 ± 0.15	3.10 ± 0.14
N_{eff}^{k5}	2.94 ± 0.24	$2.88^{+0.24}_{-0.21}$	2.94 ± 0.23	2.88 ± 0.23
N_{eff}^{k6}	$2.90^{+3.50}_{-2.90}$	$2.60^{+2.90}_{-2.50}$	$2.90^{+3.60}_{-2.90}$	$2.90^{+3.60}_{-2.80}$
N_{eff}^{k7}	★	★	★	★
H_0	$66.10^{+2.30}_{-1.30}$	$67.6^{+1.60}_{-0.89}$	$66.6^{+1.40}_{-0.97}$	$67.6^{+1.10}_{-0.80}$
Ω_m	$0.333^{+0.017}_{-0.032}$	$0.312^{+0.011}_{-0.021}$	$0.327^{+0.013}_{-0.020}$	$0.313^{+0.011}_{-0.016}$
σ_8	$0.781^{+0.036}_{-0.022}$	$0.795^{+0.027}_{-0.013}$	$0.800^{+0.020}_{-0.017}$	$0.802^{+0.019}_{-0.013}$
S_8	$0.822^{+0.013}_{-0.016}$	0.810 ± 0.013	$0.834^{+0.013}_{-0.016}$	0.818 ± 0.012

chiorri, and A. Palazzo, (2025), arXiv:2503.07752 [hep-ph].
 [4] K. Abe *et al.* (T2K), Eur. Phys. J. C **83**, 782 (2023), arXiv:2303.03222 [hep-ex].

[5] M. A. Acero *et al.* (NOvA), Phys. Rev. D **106**, 032004 (2022), arXiv:2108.08219 [hep-ex].
 [6] F. An *et al.* (JUNO), J. Phys. G **43**, 030401 (2016), arXiv:1507.05613 [physics.ins-det].

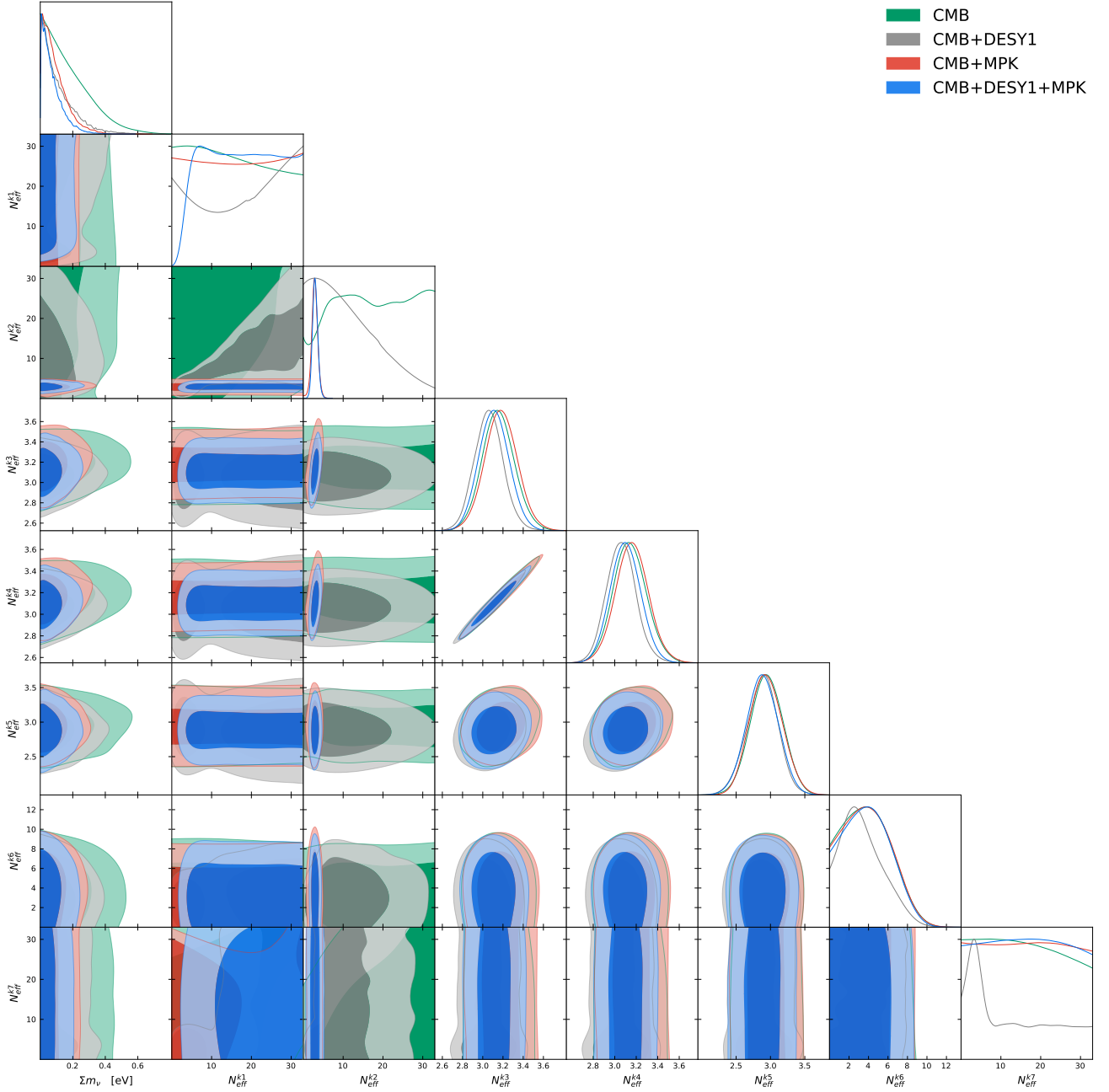


FIG. 6: One-dimensional and two-dimensional marginalized constraints on the scale-dependent number of relativistic species model with free neutrino mass from CMB, CMB plus DESY1, CMB plus MPK and CMB plus DESY1 plus MPK datasets, respectively.

- [7] K. Abe *et al.* (Hyper-Kamiokande), (2018), arXiv:1805.04163 [physics.ins-det].
- [8] B. Abi *et al.* (DUNE), (2020), arXiv:2002.03005 [hep-ex].
- [9] S. Gariazzo, M. Archidiacono, P. F. de Salas, O. Mena, C. A. Ternes, and M. Tórtola, JCAP **03**, 011 (2018), arXiv:1801.04946 [hep-ph].
- [10] M. Aker *et al.* (KATRIN), (2024), arXiv:2406.13516 [nucl-ex].
- [11] D. Wang, O. Mena, E. Di Valentino, and S. Gariazzo, (2024), arXiv:2405.03368 [astro-ph.CO].
- [12] J.-Q. Jiang, W. Giarè, S. Gariazzo, M. G. Dainotti, E. Di Valentino, O. Mena, D. Pedrotti, S. S. da Costa, and S. Vagnozzi, (2024), arXiv:2407.18047 [astro-ph.CO].
- [13] S. Hannestad, Phys. Rev. Lett. **95**, 221301 (2005), arXiv:astro-ph/0505551.
- [14] W. Yang, E. Di Valentino, S. Pan, and O. Mena, Phys. Dark Univ. **31**, 100762 (2021), arXiv:2007.02927 [astro-ph.CO].

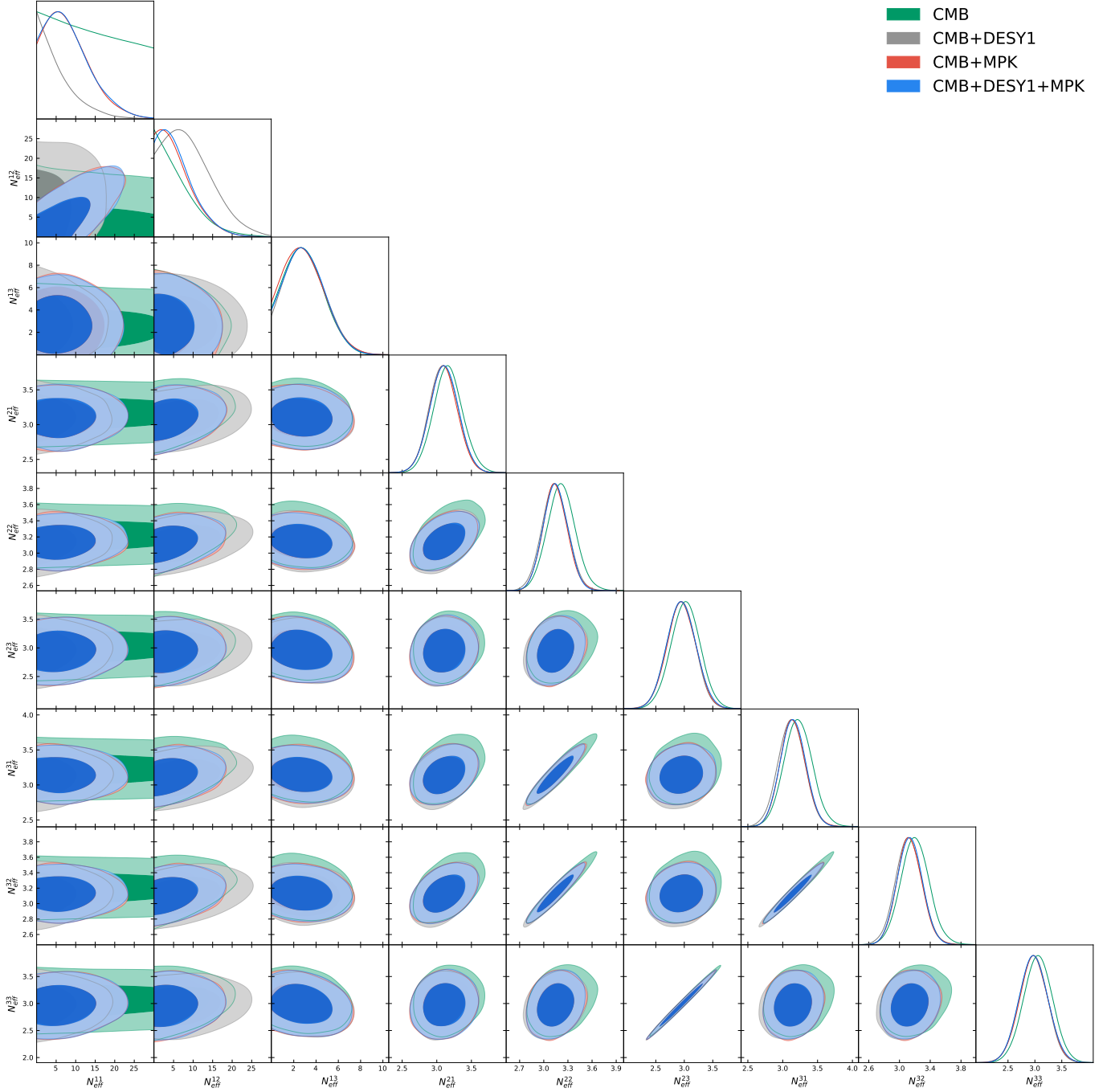


FIG. 7: One-dimensional and two-dimensional marginalized constraints on the redshift- and scale-dependent number of relativistic species model from CMB, CMB plus DESY1, CMB plus MPK and CMB plus DESY1 plus MPK datasets, respectively.

- [15] S. Vagnozzi, S. Dhawan, M. Gerbino, K. Freese, A. Goobar, and O. Mena, *Phys. Rev. D* **98**, 083501 (2018), arXiv:1801.08553 [astro-ph.CO].
- [16] S. Roy Choudhury and A. Naskar, *Eur. Phys. J. C* **79**, 262 (2019), arXiv:1807.02860 [astro-ph.CO].
- [17] E. di Valentino, S. Gariazzo, and O. Mena, *Phys. Rev. D* **106**, 043540 (2022), arXiv:2207.05167 [astro-ph.CO].
- [18] M.-M. Zhao, Y.-H. Li, J.-F. Zhang, and X. Zhang, *Mon. Not. Roy. Astron. Soc.* **469**, 1713 (2017), arXiv:1608.01219 [astro-ph.CO].
- [19] X. Zhang, *Phys. Rev. D* **93**, 083011 (2016), arXiv:1511.02651 [astro-ph.CO].
- [20] R.-Y. Guo, J.-F. Zhang, and X. Zhang, *Chin. Phys. C* **42**, 095103 (2018), arXiv:1803.06910 [astro-ph.CO].
- [21] S. Roy Choudhury and S. Hannestad, *JCAP* **07**, 037 (2020), arXiv:1907.12598 [astro-ph.CO].
- [22] H. Li and X. Zhang, *Phys. Lett. B* **713**, 160 (2012),

TABLE V: Mean values and 1σ (68%) marginalized errors of the cosmological parameters within the redshift- and scale-dependent number of relativistic species model with free neutrino mass, obtained using the CMB, CMB plus DESY1, CMB plus MPK and CMB plus DESY1 plus MPK datasets, respectively. Note that we quote 2σ (95%) limits for parameters that the data cannot constrain well. The symbols “★” denote parameters that remain unconstrained by the data.

Parameters	CMB	CMB+DESY1	CMB+MPK	CMB+DESY1+MPK
$\Omega_b h^2$	0.02242 ± 0.00019	0.02248 ± 0.00019	0.02250 ± 0.00018	0.02250 ± 0.00019
$\Omega_c h^2$	0.1222 ± 0.0026	0.1203 ± 0.0023	0.1201 ± 0.0021	0.1202 ± 0.0021
$100\theta_{MC}$	1.04068 ± 0.00042	1.04091 ± 0.00040	1.04091 ± 0.00038	1.04090 ± 0.00038
τ	0.0526 ± 0.0080	$0.0558^{+0.0074}_{-0.0083}$	$0.0546^{+0.0071}_{-0.0081}$	0.0547 ± 0.0078
$\ln(10^{10} A_s)$	3.066 ± 0.029	3.058 ± 0.028	3.057 ± 0.026	3.066 ± 0.029
n_s	0.9691 ± 0.0096	0.9676 ± 0.0094	0.9694 ± 0.0093	0.9694 ± 0.0094
N_{eff}^{11}	★	< 15.40	< 18.80	< 19.10
N_{eff}^{12}	< 16.40	< 20.20	< 14.90	< 14.80
N_{eff}^{13}	< 6.03	< 6.15	< 6.11	< 6.06
N_{eff}^{21}	3.16 ± 0.21	3.10 ± 0.20	3.10 ± 0.20	3.11 ± 0.20
N_{eff}^{22}	3.22 ± 0.18	3.14 ± 0.16	3.14 ± 0.15	3.14 ± 0.15
N_{eff}^{23}	3.02 ± 0.25	2.94 ± 0.25	2.95 ± 0.25	2.95 ± 0.25
N_{eff}^{31}	3.22 ± 0.20	3.13 ± 0.19	3.15 ± 0.18	3.15 ± 0.18
N_{eff}^{32}	3.20 ± 0.19	3.12 ± 0.17	3.13 ± 0.16	3.13 ± 0.16
N_{eff}^{33}	3.06 ± 0.27	2.97 ± 0.26	2.98 ± 0.26	2.98 ± 0.26
H_0	67.10 ± 1.00	67.87 ± 0.96	67.93 ± 0.85	67.91 ± 0.86
Ω_m	$0.322^{+0.014}_{-0.016}$	$0.310^{+0.013}_{-0.014}$	$0.309^{+0.011}_{-0.013}$	0.310 ± 0.012
σ_8	0.797 ± 0.017	0.810 ± 0.015	0.806 ± 0.014	0.806 ± 0.014
S_8	0.825 ± 0.019	0.823 ± 0.014	0.818 ± 0.012	0.818 ± 0.012

- arXiv:1202.4071 [astro-ph.CO] .
- [23] Y.-H. Li, S. Wang, X.-D. Li, and X. Zhang, JCAP **02**, 033 (2013), arXiv:1207.6679 [astro-ph.CO] .
- [24] J.-F. Zhang, Y.-H. Li, and X. Zhang, Eur. Phys. J. C **74**, 2954 (2014), arXiv:1404.3598 [astro-ph.CO] .
- [25] J.-F. Zhang, M.-M. Zhao, Y.-H. Li, and X. Zhang, JCAP **04**, 038 (2015), arXiv:1502.04028 [astro-ph.CO] .
- [26] C.-Q. Geng, C.-C. Lee, R. Myrzakulov, M. Sami, and E. N. Saridakis, JCAP **01**, 049 (2016), arXiv:1504.08141 [astro-ph.CO] .
- [27] Y. Chen and L. Xu, Phys. Lett. B **752**, 66 (2016), arXiv:1507.02008 [astro-ph.CO] .
- [28] A. Loureiro *et al.*, Phys. Rev. Lett. **123**, 081301 (2019), arXiv:1811.02578 [astro-ph.CO] .
- [29] S. Wang, Y.-F. Wang, D.-M. Xia, and X. Zhang, Phys. Rev. D **94**, 083519 (2016), arXiv:1608.00672 [astro-ph.CO] .
- [30] W. Yang, R. C. Nunes, S. Pan, and D. F. Mota, Phys. Rev. D **95**, 103522 (2017), arXiv:1703.02556 [astro-ph.CO] .
- [31] Q.-G. Huang, K. Wang, and S. Wang, Eur. Phys. J. C **76**, 489 (2016), arXiv:1512.05899 [astro-ph.CO] .
- [32] R. K. Sharma, K. L. Pandey, and S. Das, Astrophys. J. **934**, 113 (2022), arXiv:2202.01749 [astro-ph.CO] .
- [33] M. Zhang, J.-F. Zhang, and X. Zhang, Commun. Theor. Phys. **72**, 125402 (2020), arXiv:2005.04647 [astro-ph.CO] .
- [34] A. R. Khalifeh and R. Jimenez, Phys. Dark Univ. **34**, 100897 (2021), arXiv:2105.07973 [astro-ph.CO] .
- [35] Y. Chen, B. Ratra, M. Biesiada, S. Li, and Z.-H. Zhu, Astrophys. J. **829**, 61 (2016), arXiv:1603.07115 [astro-ph.CO] .
- [36] N. Aghanim *et al.* (Planck), Astron. Astrophys. **641**, A6 (2020), [Erratum: Astron. Astrophys. 652, C4 (2021)], arXiv:1807.06209 [astro-ph.CO] .
- [37] E. Giusarma, R. De Putter, and O. Mena, Phys. Rev. D **87**, 043515 (2013), arXiv:1211.2154 [astro-ph.CO] .
- [38] J.-P. Hu and F.-Y. Wang, Universe **9**, 94 (2023), arXiv:2302.05709 [astro-ph.CO] .
- [39] N. Schöneberg, G. Franco Abellán, A. Pérez Sánchez, S. J. Witte, V. Poulin, and J. Lesgourgues, Phys. Rept. **984**, 1 (2022), arXiv:2107.10291 [astro-ph.CO] .
- [40] I. G. McCarthy, S. Bird, J. Schaye, J. Harnois-Deraps, A. S. Font, and L. Van Waerbeke, Mon. Not. Roy. Astron. Soc. **476**, 2999 (2018), arXiv:1712.02411 [astro-ph.CO] .
- [41] K. N. Abazajian and A. Kusenko, Phys. Rev. D **100**, 103513 (2019), arXiv:1907.11696 [hep-ph] .

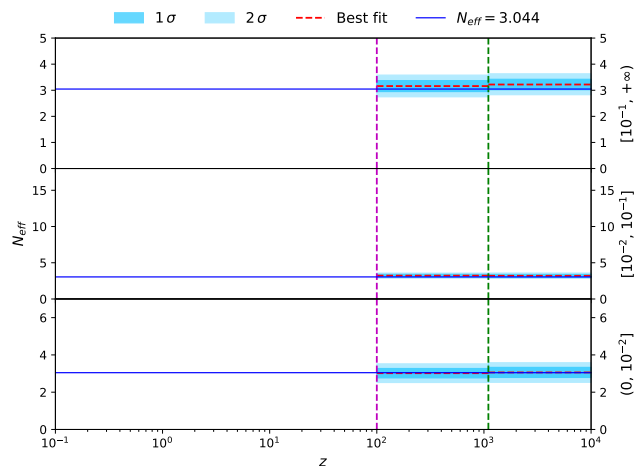


FIG. 8: The tomographic reconstruction of the redshift- and scale-dependent number of relativistic species. The blue lines denote the standard prediction of $N_{\text{eff}} = 3.044$, and the red dashed lines represent the best fit corresponding to the mean value of posterior distribution in each bin. The magenta and green vertical dashed lines describe $z = 100$ and $z = 1100$, respectively.

- [42] E. Abdalla *et al.*, *JHEAp* **34**, 49 (2022), arXiv:2203.06142 [astro-ph.CO] .
- [43] E. Di Valentino, O. Mena, S. Pan, L. Visinelli, W. Yang, A. Melchiorri, D. F. Mota, A. G. Riess, and J. Silk, *Class. Quant. Grav.* **38**, 153001 (2021), arXiv:2103.01183 [astro-ph.CO] .
- [44] L. Verde, T. Treu, and A. G. Riess, *Nature Astron.* **3**, 891 (2019), arXiv:1907.10625 [astro-ph.CO] .
- [45] L. Verde, N. Schöneberg, and H. Gil-Marín, (2023), arXiv:2311.13305 [astro-ph.CO] .
- [46] E. Di Valentino *et al.*, *Astropart. Phys.* **131**, 102604 (2021), arXiv:2008.11285 [astro-ph.CO] .
- [47] S. Roy Choudhury and S. Choubey, *JCAP* **09**, 017 (2018), arXiv:1806.10832 [astro-ph.CO] .
- [48] E. Di Valentino and A. Melchiorri, *Astrophys. J. Lett.* **931**, L18 (2022), arXiv:2112.02993 [astro-ph.CO] .
- [49] W. Giarè, O. Mena, and E. Di Valentino, *Phys. Rev. D* **108**, 103539 (2023), arXiv:2307.14204 [astro-ph.CO] .
- [50] N. Craig, D. Green, J. Meyers, and S. Rajendran, (2024), arXiv:2405.00836 [astro-ph.CO] .
- [51] D. Green and J. Meyers, (2024), arXiv:2407.07878 [astro-ph.CO] .
- [52] M. Loverde and Z. J. Weiner, (2024), arXiv:2410.00090 [astro-ph.CO] .
- [53] D. Naredo-Tuero, M. Escudero, E. Fernández-Martínez, X. Marcano, and V. Poulin, (2024), arXiv:2407.13831 [astro-ph.CO] .
- [54] I. J. Allali and A. Notari, (2024), arXiv:2406.14554 [astro-ph.CO] .
- [55] I. Esteban and J. Salvado, *JCAP* **05**, 036 (2021), arXiv:2101.05804 [hep-ph] .
- [56] I. Esteban, O. Mena, and J. Salvado, *Phys. Rev. D* **106**, 083516 (2022), arXiv:2202.04656 [astro-ph.CO] .
- [57] C. D. Kreisch, F.-Y. Cyr-Racine, and O. Doré, *Phys. Rev. D* **101**, 123505 (2020), arXiv:1902.00534 [astro-ph.CO] .
- [58] M. Lattanzi and M. Gerbino, *Front. in Phys.* **5**, 70 (2018), arXiv:1712.07109 [astro-ph.CO] .
- [59] Z. Chacko, A. Dev, P. Du, V. Poulin, and Y. Tsai, *JHEP* **04**, 020 (2020), arXiv:1909.05275 [hep-ph] .
- [60] Z. Chacko, A. Dev, P. Du, V. Poulin, and Y. Tsai, *Phys. Rev. D* **103**, 043519 (2021), arXiv:2002.08401 [astro-ph.CO] .
- [61] M. Escudero, J. Lopez-Pavon, N. Rius, and S. Sandner, *JHEP* **12**, 119 (2020), arXiv:2007.04994 [hep-ph] .
- [62] G. Franco Abellán, Z. Chacko, A. Dev, P. Du, V. Poulin, and Y. Tsai, *JHEP* **08**, 076 (2022), arXiv:2112.13862 [hep-ph] .
- [63] N. Bellomo, E. Bellini, B. Hu, R. Jimenez, C. Pena-Garay, and L. Verde, *JCAP* **02**, 043 (2017), arXiv:1612.02598 [astro-ph.CO] .
- [64] G. Dvali and L. Funcke, *Phys. Rev. D* **93**, 113002 (2016), arXiv:1602.03191 [hep-ph] .
- [65] C. S. Lorenz, L. Funcke, E. Calabrese, and S. Hannestad, *Phys. Rev. D* **99**, 023501 (2019), arXiv:1811.01991 [astro-ph.CO] .
- [66] G. Dvali, L. Funcke, and T. Vachaspati, *Phys. Rev. Lett.* **130**, 091601 (2023), arXiv:2112.02107 [hep-ph] .
- [67] C. S. Lorenz, L. Funcke, M. Löffler, and E. Calabrese, *Phys. Rev. D* **104**, 123518 (2021), arXiv:2102.13618 [astro-ph.CO] .
- [68] M. Escudero, T. Schwetz, and J. Terol-Calvo, *JHEP* **02**, 142 (2023), [Addendum: *JHEP* **06**, 119 (2024)], arXiv:2211.01729 [hep-ph] .
- [69] M. Sen and A. Y. Smirnov, *JCAP* **01**, 040 (2024), arXiv:2306.15718 [hep-ph] .
- [70] Y. Farzan and S. Hannestad, *JCAP* **02**, 058 (2016), arXiv:1510.02201 [hep-ph] .
- [71] J. Alvey, M. Escudero, N. Sabti, and T. Schwetz, *Phys. Rev. D* **105**, 063501 (2022), arXiv:2111.14870 [hep-ph] .
- [72] I. M. Oldengott, G. Barenboim, S. Kahlen, J. Salvado, and D. J. Schwarz, *JCAP* **04**, 049 (2019), arXiv:1901.04352 [astro-ph.CO] .
- [73] J. Alvey, M. Escudero, and N. Sabti, *JCAP* **02**, 037 (2022), arXiv:2111.12726 [astro-ph.CO] .
- [74] A. Cuoco, J. Lesgourgues, G. Mangano, and S. Pastor, *Phys. Rev. D* **71**, 123501 (2005), arXiv:astro-ph/0502465 .
- [75] I. J. Allali, D. Aloni, and N. Schöneberg, *JCAP* **09**, 019 (2024), arXiv:2404.16822 [astro-ph.CO] .
- [76] C. Benso, T. Schwetz, and D. Vatsyayan, (2024), arXiv:2410.23926 [hep-ph] .
- [77] T. Bertólez-Martínez, I. Esteban, R. Hajjar, O. Mena, and J. Salvado, (2024), arXiv:2411.14524 [astro-ph.CO] .
- [78] S. Gariazzo, P. F. de Salas, and S. Pastor, *JCAP* **07**, 014 (2019), arXiv:1905.11290 [astro-ph.CO] .
- [79] S. Gariazzo, P. Martínez-Miravé, O. Mena, S. Pastor, and M. Tórtola, *JCAP* **03**, 046 (2023), arXiv:2211.10522 [hep-ph] .
- [80] K. Akita and M. Yamaguchi, *JCAP* **08**, 012 (2020), arXiv:2005.07047 [hep-ph] .
- [81] J. Froustey, C. Pitrou, and M. C. Volpe, *JCAP* **12**, 015 (2020), arXiv:2008.01074 [hep-ph] .
- [82] J. J. Bennett *et al.*, *JCAP* **04**, 073 (2021), arXiv:2012.02726 [hep-ph] .
- [83] M. Cielo, M. Escudero, G. Mangano, and O. Pisanti, *Phys. Rev. D* **108**, L121301 (2023), arXiv:2306.05460

- [hep-ph] .
- [84] M. Drewes, Y. Georis, M. Klasen, L. P. Wiggering, and Y. Y. Wong, (2024), arXiv:2402.18481 [hep-ph] .
- [85] G. Mangano, G. Miele, S. Pastor, T. Pinto, O. Pisanti, and P. D. Serpico, Nucl.Phys. **B729**, 221 (2005), arXiv:hep-ph/0506164 [hep-ph] .
- [86] P. F. de Salas and S. Pastor, JCAP **07**, 051 (2016), arXiv:1606.06986 [hep-ph] .
- [87] R. Consiglio, P. F. de Salas, G. Mangano, G. Miele, S. Pastor, and O. Pisanti, Comput.Phys.Commun. **233**, 237 (2018), arXiv:1712.04378 [astro-ph.CO] .
- [88] S. Safi, M. Farhang, O. Mena, and E. Di Valentino, Phys. Rev. D **110**, 103513 (2024), arXiv:2404.01457 [astro-ph.CO] .
- [89] M. Archidiacono *et al.* (Euclid), (2024), arXiv:2405.06047 [astro-ph.CO] .
- [90] A. Aghamousa *et al.* (DESI), (2016), arXiv:1611.00036 [astro-ph.IM] .
- [91] P. Ade *et al.* (Simons Observatory), JCAP **02**, 056 (2019), arXiv:1808.07445 [astro-ph.CO] .
- [92] E. Allys *et al.* (LiteBIRD), PTEP **2023**, 042F01 (2023), arXiv:2202.02773 [astro-ph.IM] .
- [93] N. Aghanim *et al.* (Planck), Astron. Astrophys. **641**, A5 (2020), arXiv:1907.12875 [astro-ph.CO] .
- [94] N. Aghanim *et al.* (Planck), Astron. Astrophys. **641**, A8 (2020), arXiv:1807.06210 [astro-ph.CO] .
- [95] N. Aghanim *et al.* (Planck), Astron. Astrophys. **641**, A1 (2020), arXiv:1807.06205 [astro-ph.CO] .
- [96] <https://pla.esac.esa.int>, .
- [97] C. Blake *et al.*, Mon. Not. Roy. Astron. Soc. **406**, 803 (2010), arXiv:1003.5721 [astro-ph.CO] .
- [98] D. Parkinson *et al.*, Phys. Rev. D **86**, 103518 (2012), arXiv:1210.2130 [astro-ph.CO] .
- [99] T. M. C. Abbott *et al.* (DES), Phys. Rev. D **98**, 043526 (2018), arXiv:1708.01530 [astro-ph.CO] .
- [100] J. Prat *et al.* (DES), Phys. Rev. D **98**, 042005 (2018), arXiv:1708.01537 [astro-ph.CO] .
- [101] J. Elvin-Poole *et al.* (DES), Phys. Rev. D **98**, 042006 (2018), arXiv:1708.01536 [astro-ph.CO] .
- [102] M. A. Troxel *et al.* (DES), Phys. Rev. D **98**, 043528 (2018), arXiv:1708.01538 [astro-ph.CO] .
- [103] T. M. C. Abbott *et al.* (DES), Phys. Rev. D **99**, 123505 (2019), arXiv:1810.02499 [astro-ph.CO] .
- [104] A. Lewis, A. Challinor, and A. Lasenby, Astrophys. J. **538**, 473 (2000), arXiv:astro-ph/9911177 .
- [105] A. Lewis and S. Bridle, Phys. Rev. D **66**, 103511 (2002), arXiv:astro-ph/0205436 .
- [106] A. Lewis, Phys. Rev. D **87**, 103529 (2013), arXiv:1304.4473 [astro-ph.CO] .
- [107] A. Gelman and D. B. Rubin, Statist. Sci. **7**, 457 (1992).
- [108] A. Lewis, (2019), arXiv:1910.13970 [astro-ph.IM] .
- [109] D. Wang and O. Mena, (2024), arXiv:2402.18248 [astro-ph.CO] .